The Annual Modes of Tropical Precipitation Simulated by the LASG/IAP Coupled Ocean-Atmosphere Model FGOALS_s1.1*

ZHANG Lixia[1,2†](张丽霞), ZHOU Tianjun[1](周天军), WU Bo[1] (吴 波), and BAO Qing[1](包 庆)

1 *LASG, Institute of Atmospheric Physics, Chinese Academy of Sciences, Beijing* 100029

2 *Graduate University of Chinese Academy of Sciences, Beijing* 100049

(Received July 1, 2009)

ABSTRACT

This paper evaluates the performance of a coupled general circulation model FGOALS_s1.1 developed by LASG/IAP in simulating the annual modes of tropical precipitation. To understand the impacts of air-sea coupling on the annual modes, the result of an off-line simulation of the atmospheric component of FGOALS_s1.1, i.e., LASG/IAP atmospheric general circulation model SAMIL, is also analyzed.

FGOALS_s1.1 can reasonably reproduce major characteristics of the annual mean precipitation. Nonetheless, the coupled model shows overestimation of precipitation over the equatorial Pacific and tropical South Pacific, and underestimation of precipitation over the northern equatorial Pacific. The monsoon mode simulated by FGOALS_s1.1 shows an equatorial anti-symmetric structure, which is consistent with the observation. The bias of the coupled model in simulating monsoon mode resembles that of SAMIL, especially over the subtropics. The main deficiency of FGOALS_s1.1 is its failure in simulating the spring-fall asymmetric mode. This is attributed to the false phase of sea surface temperature anomaly (SSTA) annual cycle over the equatorial central-eastern Pacific and Indian Ocean, which leads to the bias of the Walker circulation over the equatorial Pacific and the anti-Walker circulation over the Indian Ocean in boreal spring and fall. In addition, the domains of the western North Pacific monsoon and Indian monsoon simulated by the coupled model are smaller than the observation. The study suggests that the bias of the fully coupled ocean-atmosphere model can only be partly attributed to the bias of the atmospheric component. The performance of FGOALS_s1.1 in simulating the annual cycle of equatorial SST deserves further improvement.

Key words: climate system model, annual modes of precipitation, global monsoon

Citation: Zhang Lixia, Zhou Tianjun, Wu Bo, et al., 2010: The annual modes of tropical precipitation simulated by the LASG/IAP coupled ocean-atmosphere model FGOALS_s1.1. *Acta Meteor. Sinica*, **24**(2), 189–202.

1. Introduction

The annual variation of the solar radiation induces a significant reversal of temperature gradient between the Northern and Southern Hemisphere and temperature contrast between land and adjacent oceans, which further drives the annual variation of the global general circulation. Although the sun crosses the equator twice a year, an annual harmonic is dominant in the equatorial atmosphere and ocean (Wyrtki and Mayers, 1976; Horel, 1982; Hasternrath and Lamb, 1978; Lau and Sheu, 1988; Gadgil and Asha, 1992; Ferranti et al., 1997). Here we focus on the tropical precipitation, which plays an important role in driving the general circulation and hydrological cycle, as well as in linking external radiative forcing and the atmospheric circulation.

There are many studies about the annual variation of precipitation. The earliest studies mostly examined the annual cycle of global precipitation in the concept of hemispheric mean (Jaeger, 1983; Peizoto and Oort, 1983). Chen et al. (1995) studied the annual variations of the global atmospheric hydrological process, and found that it origins from the tropical-subtropical region. Later, Zhou et al. (1999) found that the subtropical oceans act as important moisture sources in the water vapor transport and the fresh water exchange between air and sea. The annual variation of precipitation along storm tracks in both hemispheres follows that of the convergence

*Supported by the National Natural Science Foundation of China under Grant Nos. 40625014, 40628006, and 40523001, and the China Meteorological Administration under Grant Nos. GYHY200706005 and GYHY200706010.

†Corresponding author: lixiazhang@mail.iap.ac.cn.

(Chinese version published in Vol. 66, No. 6, 2008)

of transient water vapor flux (Chen et al., 2004).

The study about monsoon precipitation is the focus of climate research. Compared with other areas, the variation of monsoon precipitation is significant on many timescales (e.g., intraseasonal, interannual, and interdecadal) (Fu and Zeng, 1997). The monsoon rainfall accounts for 31% of the global precipitation variance. Previous monsoon studies primarily focused on one monsoon region or monsoon system and identified individual monsoon region through special definition (Chase et al., 2003; Krispalani et al., 2003; Jones et al., 2004; Schreck and Semazzi, 2004; Yu and Zhou, 2007). However, we know that all regional monsoons are coordinated by the annual cycle of solar radiation and thus connected with each other. For instance, there are some connections between southern Asian and Australian monsoons (Meehl, 1987), between southern American and African monsoons (Biasutti et al., 2003), between East Asian-western North Pacific and North American monsoons (Wang et al., 2001; Lau and Weng, 2002). Dai et al. (2002) found an Indian-East-Asian (IEA) teleconnection pattern.

The close relationships among different monsoon systems inspire us to examine the change of global monsoon as a whole. The global monsoon system should be seen as the persistent global-scale overturning of the atmosphere that varies with the time of year (Trenberth et al., 2000). Wang and Ding (2008) extracted two major modes of annual variation using a multi-variable EOF (MV-EOF) analysis of 12-mon climatological precipitation and 850-hPa wind, which are termed as monsoon mode and spring-fall asymmetric mode. The two dominant modes can be seen as new objective standards for gauging the performance of climate models in the simulation of the mean state and annual cycle. Recently, Zhou et al. (2008a) revealed the forcing role of the tropical sea surface temperature (SST) on global monsoon rainfall through atmospheric general circulation model driven by historical SST.

Climate system model is a useful tool for understanding climate variability and predicting climate change. Recently, a fully coupled atmosphere-land-sea-ice climate model FGOALS (flexible global ocean-atmosphere-land system) is developed in the State Key Laboratory of Numerical Modeling for Atmospheric Sciences and Geophysical Fluid Dynamics (LASG), Institute of Atmospheric Physics (IAP). The FGOALS has two versions, i.e., FGOALS_s and FGOALS_g, which employ spectral atmospheric model (SAMIL) and grid atmospheric model (GAMIL) as their atmospheric component respectively. There are many evaluations about FGOALS_g (Zhou and Yu, 2006; Zhou et al., 2008c; Dai, 2006). However, the analysis about the simulation of FGOALS_s is quite few. Wang et al. (2007) evaluated the performance of SAMIL and FGOALS_s, and found that FGOALS_s improved the performance of precipitation simulations in boreal winter and summer. The annual cycle of precipitation in the model is still unknown. This paper aims to evaluate the performance of FGOALS_s1.1 (hereafter FGOALS_s) in simulating the annual cycle of tropical precipitation, and to reveal the causes model biases.

2. Models and methodology

2.1 Models and data

The model used in this study is FGOALS_s. The atmosphere, ocean, land, and ice components are coupled by NCAR CPL5. The atmosphere component is SAMIL, which is a spectral AGCM developed in IAP/LASG (Bao et al., 2006). SAMIL is rhomboidally truncated at zonal wave number 42, roughly equivalent to a horizontal resolution of 2.81° (longitude)×1.66° (latitude), and has 26 vertical layers with a top at 2.1941 hPa, named R42L26. The ocean component is the LICOM, which is based on the third generation of the LASG/IAP ocean general circulation model L30T63 (Jin et al., 1999; Liu et al., 2004). The LICOM has a horizontal resolution of 1°×1° (longitude×latitude) and 30 vertical layers. The land and ice components are CLM2 (Vertenstein et al., 2002) and CSIM4, respectively (Briegleb et al., 2002). There is no correction in the heat and freshwater fluxes exchange at the interfaces among the atmosphere, ocean, sea ice, and land during coupled integrations. More details about FGOALS_s can be found in Zhou et al. (2005a).

A two hundred-year fully coupled run was performed. Monthly data of the 191–200th model year are analyzed in this study. In order to discuss the impacts of ocean-atmosphere coupling and the model bias, the output of SAMIL driven by the historical SST from 1980 to 1989 is also analyzed (Zhou et al., 2005b). The following data are used as "observational" evidence for evaluating the model: (1) monthly precipitation data of CPC merged analysis of precipitation (CMAP) (Xie and Arkin, 1997); (2) monthly sea surface temperature data of from GISST sea ice and SST) for the period 1980–1989 (Rayner et al., 1996); and (3) NCEP/NCAR reanalysis data (Kalnay et al., 1996).

2.2 Methodology

Through performing MV-EOF analysis on climatological precipitation and wind at 850 hPa, Wang and Ding (2008) (hereafter WD2008) found that the first two leading modes bear characteristics of the annual cycle, and account for 71% and 13% of the annual variance, respectively. The first leading mode (AC1) is monsoon mode, whose spatial pattern is close to the June-September (JJAS) ($\mathrm{Pr_{JJAS}}$) minus December-March (DJFM) ($\mathrm{Pr_{DJFM}}$) precipitation pattern, reflecting the impact of the antisymmetric solar radiation forcing. The second mode (AC2) is the spring-fall asymmetric mode. Its spatial pattern resembles the April-May (AM) ($\mathrm{Pr_{AM}}$) minus October-November (ON) ($\mathrm{Pr_{ON}}$) precipitation pattern. They can be depicted as follows:

$$\mathrm{AC1} = \mathrm{Pr_{JJAS}} - \mathrm{Pr_{DJFM}}, \quad (1)$$

$$\mathrm{AC2} = \mathrm{Pr_{AM}} - \mathrm{Pr_{ON}}. \quad (2)$$

The solar radiation flux at the surface under clear skies can be decomposed into a symmetric and an antisymmetric component about the equator (Wang, 1994). The antisymmetric component is attributed to the seasonal variation of solar declination angle. The monsoon mode represents the antisymmetric component. The spring-fall asymmetric mode represents the asymmetry of rainfall between spring and fall. It is an important feature of tropical circulation, especially the asymmetric location of ITCZ in transitional season. Chang et al. (2005) attributed it to the asymmetric wind-terrain interaction and low level divergence asymmetry, both of which are induced by land-ocean interaction. However, the analysis mainly focused on the Eastern Hemisphere. In terms of the global scale, Webster et al. (1998) proposed that it is related to the asymmetric strength of Walker circulation between boreal spring and fall.

Based on the annual modes, WD2008 proposed a concept of global monsoon. The global monsoon domain can be delineated by a simple monsoon precipitation index (MPI), which is the local annual range of precipitation (May-September (MJJAS) minus November-March (NDJFM) in the Northern Hemisphere, and NDJFM minus MJJAS in the Southern Hemisphere) normalized by the annual mean precipitation, i.e.,

In the Northern Hemisphere:

$$\mathrm{MPI} = (\mathrm{Pr_{MJJAS}} - \mathrm{Pr_{NDJFM}})/(\text{annual mean}). \quad (3)$$

While in the Southern Hemisphere:

$$\mathrm{MPI} = (\mathrm{Pr_{NDJFM}} - \mathrm{Pr_{MJJAS}})/(\text{annual mean}), \quad (4)$$

where $\mathrm{Pr_{MJJAS}}$ and $\mathrm{Pr_{NDJFM}}$ represent the total precipitation from March to September and November to May, respectively. Annual mean denotes the annual mean precipitation. The monsoon domains are the areas where annual range of precipitation exceeds 300 mm and MPI exceeds 0.5. It not only reflects the wet-dry contrast, but also represents the ratio of seasonal variation. Hence, it is a comprehensive index. The domains are quite consistent with other two definitions made by Wang and Lin (2002) and Wang and Ding (2006).

3. Results

3.1 Annual mean precipitation

The geographical distributions of climatological annual mean precipitation from observation and models are shown in Fig. 1. In the observation, major precipitation belts are located over the intertropical convergence zone (ITCZ), South Pacific convergence zone (SPCZ), equatorial Africa, western North Pacific Ocean, as well as North Africa and southern America

adjacent to the ITCZ. The precipitation pattern exhibits remarkable longitudinal and latitudinal asymmetries (Annamalai et al., 1999).Major precipitation belts are reproduced by the CGCM. However, biases are also evident (Fig. 1d). The CGCM overestimates precipitation over the equatorial North Pacific, South China Sea, western Indian Ocean, and southeastern part of South America. The excessive precipitation in the equatorial northern Pacific is associated with the northward shift of the ITCZ in FGOALS_s. The underestimation of precipitation is seen over the mid-latitude and Pacific warm pool regions. The bias over East Asia is less than 0.5 mm day^{-1}, indicating that the model performs better over this region.

To reveal the origin of the coupled model biases, we analyzed the annual mean precipitation simulated by stand-alone atmospheric component, i.e., SAMIL (Fig. 1c). Over land regions, the biases of SAMIL resemble that of FGOALS_s (Fig. 1e). In contrast, over oceans, the differences of biases between SAMIL and FGOALS_s are remarkable. For instance, the biases of SAMIL over the equatorial western Pacific and the Bay of Bengal are opposite to that of FGOALS_s. Therefore, the atmospheric component should not be the only origin of the biases of the coupled model. The air-sea coupling process may also contribute to the biases. The simulated SST biases are shown in Fig. 1d. Previous analysis showed that the SST of the coupled model is colder than the observation (Zhou et al., 2005b). The colder SST is consistent with the deficient rainfall bias (Fig. 1f).

In order to quantitatively assess the performance of the models, the root-mean-square error (RMSE) and pattern correlation coefficient (PCC) between the observed and simulated seasonal mean precipitation fields are calculated and shown in a Taylor diagram (Fig. 2; Taylor, 2001). The RMSE of FGOALS_s (1.69) is smaller than that of SAMIL (2.43) in JJA, but larger (1.79) than that of SAMIL (1.34) in MAM. The PCCs of FGOALS_s are lower than that of SAMIL in MAM, while larger than that in DJF and SON. In terms of PCC, there is no obvious improvement in the boreal summer rainfall. The RMSE and PCC of annual mean (AM) rainfall simulated by the two models are comparable. The above results suggest that the air-sea coupling improves the precipitation simulation in boreal fall and summer, but impacts less in boreal spring.

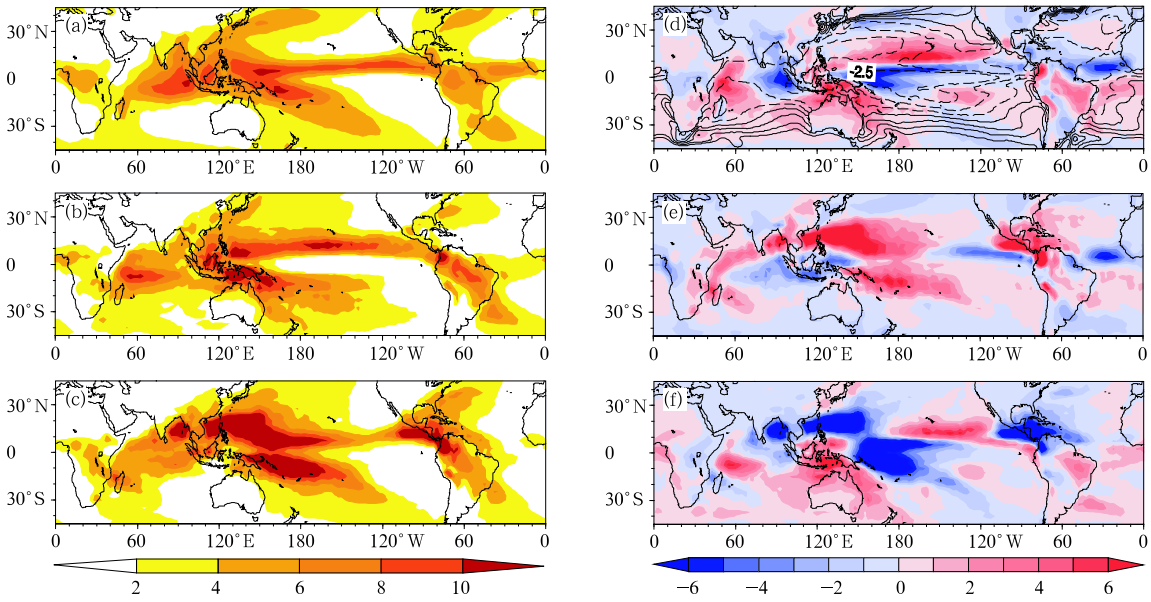

Fig. 1. Spatial patterns of long-term annual mean precipitation from (a) CMAP, (b) FGOALS_s, (c) SAMIL, and mean bias defined as the difference of precipitation (shadings) or SST (contours) between FGOALS_s and CMAP, (e) SAMIL and CMAP, and (f) FGOALS_s and SAMIL (unit of precipitation: mm day^{-1}; unit of SST bias: °C).

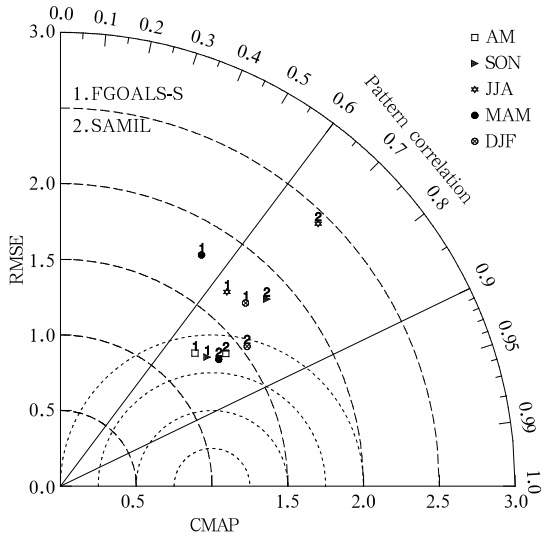

Fig. 2. Pattern statistics describing the seasonal precipitation of FGOALS_s and SAMIL compared with the observation. The isoclines indicate pattern correlation coefficient (PCC) and root-mean-square error (RMSE).

3.2 Annual cycle modes

In terms of Eq. (1), the observed and simulated monsoon modes are obtained (Fig. 3). FGOALS_s reasonably reproduces the antisymmetric pattern, i.e., the positive precipitation anomalies in East Asia, North America, and North Africa, and the negative precipitation anomalies in South Africa, Australia, and South America (Figs. 3a, b). However, the model deficiencies are also evident. Firstly, the positive pattern in the northwestern Pacific Ocean shifts northward and the positive precipitation area in India is smaller than that in the observation. Secondly, the simulated precipitation anomaly is weaker in the Bay of Bengal, but stronger in Southeast China-Meiyu band and midlatitude of North Pacific (Fig. 3e). The precipitation anomalies over the South China Sea, Philippine Sea, equatorial North Pacific, and East Indian Ocean are also underestimated. Negative biases dominate the whole extratropical continent except for North Africa. Note that the Southern Hemisphere is dominated by negative biases, which intensifies the monsoon mode. Therefore, the strength of the summer monsoon in the Southern Hemisphere is overestimated. The biases over extra-equatorial areas of the two models resemble each other. The major discrepancies are salient over the equatorial southern Africa, northwestern Australia, equatorial Pacific Ocean, and central North America. This may be associated with the simulated SST bias in FGOALS_s.

To investigate the model skill in simulating the seasonal cycle of the monsoon mode, principal

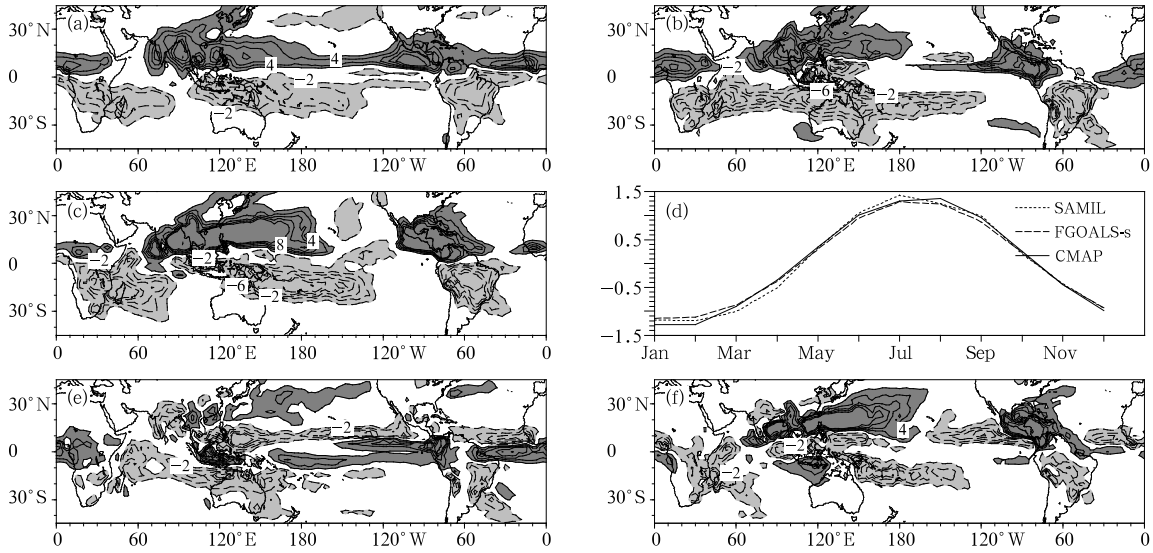

Fig. 3. The leading mode of tropical precipitation from (a) CMAP, (b) FGOALS_s, and (c) SAMIL. Principal component time series (d) of the leading mode from CMAP, FGOALS_s, and SAMIL. The differences between the leading modes of (e) FGOALS_s and CMAP, (f) SAMIL and CMAP. The darkly shaded areas indicate positive values, and lightly shaded negative values (unit: mm day^{-1}).

component time series for the first mode is obtained through applying empirical orthogonal function (EOF) analysis on the climatological monthly mean precipitation (Fig. 3d). In the observation, the PC1 reaches its maximum in boreal summer and minimum in boreal winter. These characteristics of the temporal evolution are reasonably simulated by FGOALS_s and SAMIL.

The second annual cycle mode, i.e., the spring-fall asymmetric mode, is reproduced by FGOALS_s and SAMIL (Figs. 4a-c), but with less fidelity compared with the monsoon mode. The coupled model reproduces the negative pattern in northern Pacific and the positive pattern in the Indian Ocean and East Asia. The spatial pattern in southern America and Africa simulated by the CGCM is close to the observation. The major biases of FGOALS_s (Fig. 4e) are listed as follows: firstly, the equatorial zone is dominated by negative bias except the maritime continent, while the extra-equatorial Pacific and Atlantic is covered by significant positive bias. The biases are associated with the bias of SST annual cycle, which will be discussed later. Secondly, the strength of spring-fall asymmetry mode over the Northern Hemisphere continent is underestimated, that is, the intensity of the simulated spring-fall asymmetry over the northern Pacific, Atlantic and Indian Ocean is weaker than the observation. The positive mode over ITCZ and eastern South Africa is well simulated by SAMIL, but is absent in the coupled model. Therefore, the spring-fall asymmetry is not significant over the equator in FGOALS_s. In addition, the major discrepancies over the extra-equatorial region in the two models are analogous (Figs. 4e, f).

Figure 4d shows the second principal component (PC2) of the observation and models. In the observation, the PC2 reaches the maximum (minimum) in October (April). In general, the seasonal variations of the PC2 in the two models are close to that of the observation, but with less fidelity compared with the simulated PC1.

The RMSE and PCC are also calculated to measure the performance of models (Table 1). The RMSE and PCC of AC1 are comparable to the annual mean precipitation in FGOALS_s, but the skill of AC2 is lower. The SAMIL is better than FGOALS_s in simulating the spring-fall asymmetry mode in terms of RMSE and PCC. The reason for the deficiency of FGOALS_s in simulating the spring-fall asymmetry mode will be discussed in Section 4.

3.3 Monsoon domain

According to Eqs. (3) and (4), the distributions of precipitation annual range (shaded) and monsoon domain (contours) are obtained and shown in Fig. 5. The precipitation annual range is used to measure the

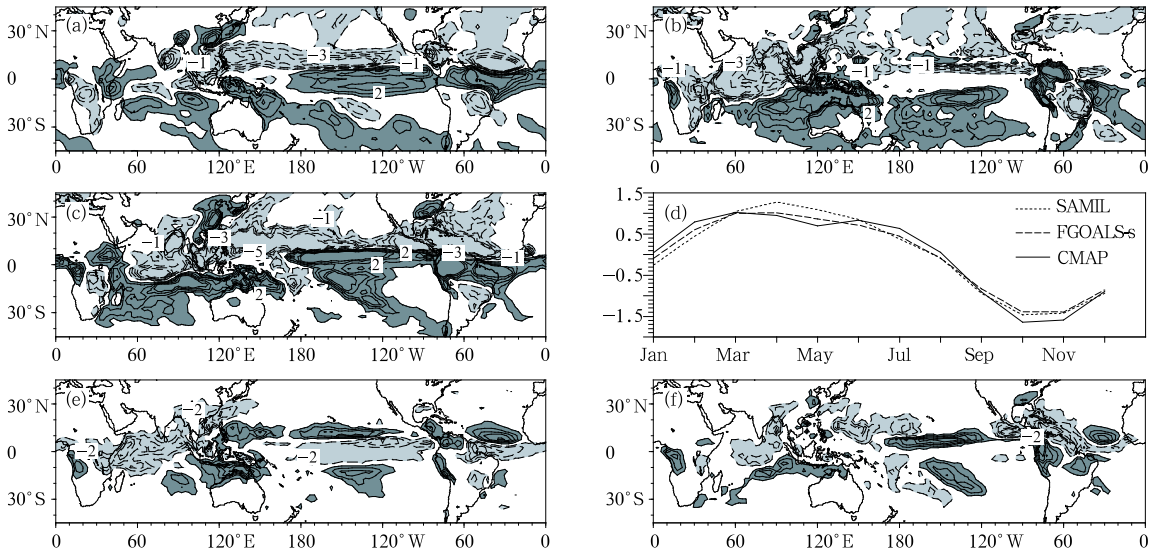

Fig. 4. As in Fig. 3, but for the second mode.

Table 1. The pattern correlation coefficient (PCC) and root-mean-square error (RMSE) between simulated and observed annual cycle modes

		PCC	RMSE
AC1	FGOALS_s	0.65	2.07
	SAMIL	0.75	2.58
AC2	FGOALS_s	0.35	1.72
	SAMIL	0.58	1.68

monsoon intensity. The FGOALS_s (Fig. 5b) realistically reproduces major monsoon domains (Fig. 5a), including the Asian-Australian monsoon, North and South African monsoon, and North and South American monsoon. The Asian monsoon and western North Pacific monsoon domains of FGOALS_s are smaller than those in the observation, while the South African monsoon and Australian monsoon domains are larger. In addition, the simulated western North Pacific monsoon shifts northward. In SAMIL, the simulated North African and Australian monsoon domains are smaller and all the regional monsoon intensities are stronger than those in the observation. FGOALS_s shows a clear improvement relative to SAMIL in simulating the strength and domain of the South Indian, Southwest Pacific Ocean, and North American monsoons, implying the important role of air-sea coupling in the monsoon simulation. However, the CGCM also exhibits apparent biases. For instance, the Asian monsoon and western North Pacific monsoon domains are smaller than the observation, and the South African monsoon and Australian monsoon domains are connected together.

3.4 Annual cycle of each regional monsoon

Following Zhou et al. (2008b), the global monsoon is divided into eight regional monsoons, including East Asian monsoon (20°–45°N, 105°–160°E), Indian monsoon (5°–30°N, 60°–105°E), western North Pacific monsoon (5°–20°N, 105°–160°E), Australian monsoon (20°–5°S, 105°–160°E), North American monsoon (0°–45°N, 120°–60°W), South American monsoon (30°S–0°, 120°–60°W), North African monsoon (0°–25°N, 60°W–60°E), and South African monsoon (30°S–0°, 60°W–60°E). The climatological monthly

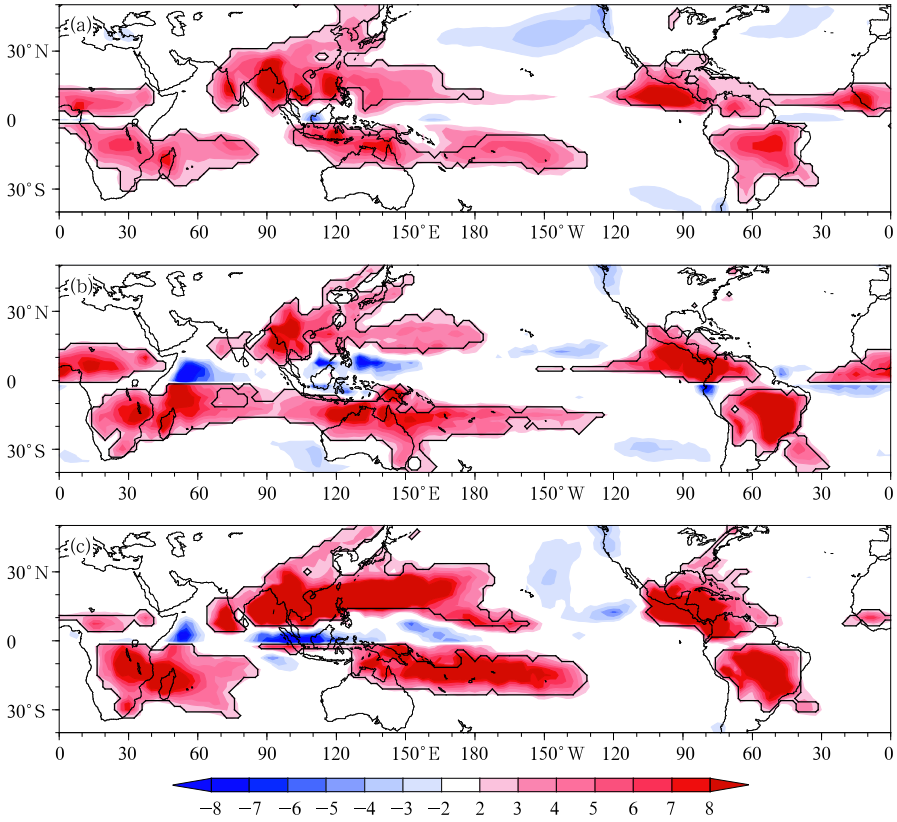

Fig. 5. Observed and simulated annual ranges of precipitation from (a) CMAP, (b) FGOALS_s, and (c) SAMIL. Bold lines indicate the global monsoon domain.

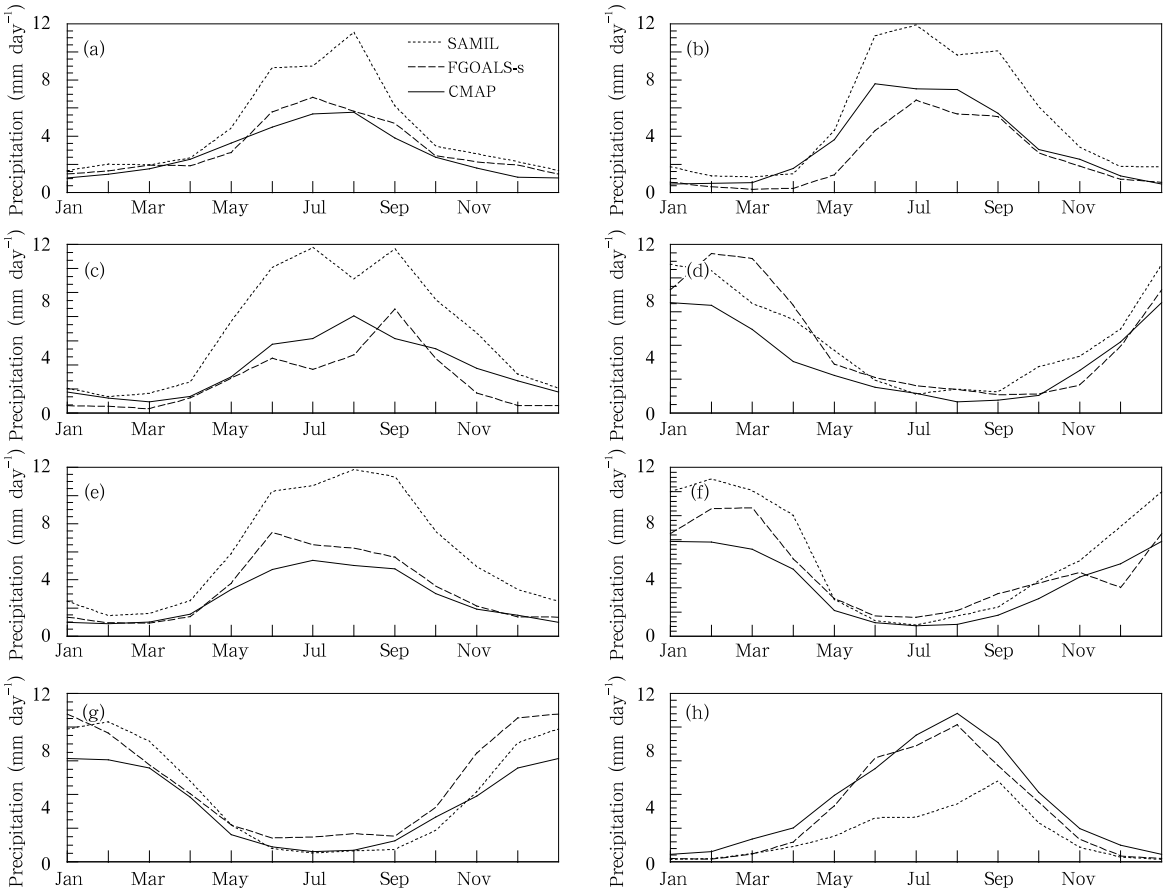

Fig. 6. Time series of climatological monthly mean precipitation (mm day^{-1}) averaged over domains of (a) East Asian monsoon, (b) Indian monsoon, (c) western North Pacific monsoon, (d) Australian monsoon, (e) North American monsoon, (f) South American monsoon, (g) South African monsoon, and (h) North African monsoon.

area-averaged precipitation in each regional monsoon is shown in Fig. 6.

The two models reasonably reproduce the climatological annual variation of each regional monsoon (Fig. 6). The intensities of summer precipitation of all regional monsoons in FGOALS_s are weaker than in SAMIL, except North African monsoon. Compared with SAMIL, the rainfall intensities of the East Asian monsoon, North American monsoon, and North African monsoon simulated by FGOALS_s are closer to the observation. The correlation coefficients between the observation and simulations are shown in Table 2. SAMIL is well correlated with the observation than FGOALS_s for almost all regional monsoons, except the Indian monsoon. Therefore, although simulations of the monsoon domain coverage exhibit somewhat improvement in the CGCM, its performance in simulating the climatological monthly area-averaged rainfall of each regional monsoon is instead worse than that in the SAMIL.

Table 2. The correlation coefficient between simulated and observed precipitation annual cycles in different monsoon domains

	East Asia	India	Western North Pacific	Australia	North America	South America	South Africa	North Africa
FGOALS_s	0.96	0.93	0.83	0.90	0.98	0.92	0.96	0.99
SAMIL	0.97	0.97	0.93	0.98	0.98	0.99	0.99	0.93

4. Discussion

As demonstrated in Section 3.2, the spring-fall asymmetry mode in FGOALS_s shows less fidelity than that in SAMIL. The existence of the spring-fall asymmetry mode is caused by the different strengths

of Walker circulation in boreal spring and fall (Webster et al., 1998).

The longitude-height diagrams of vertical velocity for the equatorial belt (averaged over 5°S–5°N) in boreal spring and fall are shown in Fig. 7. In the observation, both the ascending motions over the Pacific warm pool and eastern Atlantic Ocean and the descending motions over the western Indian Ocean and Pacific cold tongue region are weaker in spring (Fig. 7a) than in fall (Fig. 7d), indicating that the Walker circulation is stronger in boreal fall than in boreal spring.

Many previous studies indicated that Walker circulation is driven by the zonal SST gradients (Wang, 1994; Li and Philander, 1996). Since the SST in the equatorial Central Pacific is warmer in boreal spring than in fall, the zonal SST gradient across the equatorial Pacific Ocean is stronger in fall than in spring. The stronger SST gradient drives stronger local Walker circulation in fall. As a result, the spring-fall asymmetry mode forms.

FGOALS_s well reproduces the locations of ascending/descending motions (Figs. 7b, e). However, the biases in intensity reduce the simulation skill of the spring-fall asymmetric mode. Compared with the observation, FGOALS_s (Fig. 7b) shows stronger ascending motion over the warm pool (120°E), and stronger subsidence over the western Indian Ocean (60°E) and eastern Pacific Ocean (180°–120°W) in boreal spring, indicating that Walker circulation in FGOALS_s is stronger than in the observation. In boreal fall, although the intensities of ascending motion over the Pacific warm pool and the subsidence over the eastern Pacific Ocean are comparable to the observation, the subsidence over the western Indian Ocean is much weaker than the observation. Therefore, the Walker circulation in the FGOALS_s is weaker than the observation in fall. The combination of the stronger Walker circulation in spring and the weaker one in fall leads to a weaker spring-fall asymmetric mode over equatorial band and further results in the poor performance of FGOALS_s in the simulation of the second mode. Although there are some biases in the vertical motion, the performance of SAMIL is generally better than the FGOALS_s, especially in boreal spring. This is associated with the true lower boundary forcing in the AMIP run.

To further investigate the relationship between the AC2 and the underlying SST, spatial distributions of correlations between the observed and simulated PC2 and the climatological monthly mean SST are shown in Fig. 8. In the observation (Fig. 8a), significant positive correlation coefficients are seen over the Indian Ocean, South Pacific, South Atlantic, and equatorial eastern Pacific, while negative correlation coefficients are seen in the Pacific and Atlantic Ocean in the Northern Hemisphere. Antisymmetry about the equator exists in the Pacific and Atlantic Ocean. The FGOALS_s reasonably reproduces the antisymmetry over the Pacific and Atlantic Ocean (Fig. 8b). However, the simulated correlation coefficient is opposite to the observation in the northern Indian Ocean and maritime continent. In addition, the FGOALS_s has an unrealistic positive center over the eastern equatorial Pacific. The spatial patterns of SAMIL resemble those of the observation (Fig. 8c). Since the PC2 of FGOALS_s resembles the observation (Fig. 4d), the poor performance of FGOALS_s in simulating the spring-fall asymmetric mode is primarily caused by the bias of the SST annual cycle.

To support this hypothesis, we check the annual cycle of equatorial SST anomalies (SSTA), which are the departures of climatologically monthly mean from the long-term mean for the equatorial belt (average of 5°S–5°N) (Fig. 9). In the observation, the SSTA over the equatorial eastern Pacific, Atlantic and Indian Ocean undergoes an obvious annual cycle with the cold phase peaking in July-September and the warm phase in March and April (Wyrtki, 1965; Hastenrath and Heller, 1977; Merle et al., 1980; Picaut, 1983). A semi-annual cycle dominates the western Pacific. The FGOALS_s (Fig. 9b) reproduces the warm phase in March-May and the cold phase in June-September over the western Pacific Ocean, but it fails to capture the semi-annual cycle over the western Pacific, and it has an opposite annual cycle in the Indian Ocean, eastern equatorial Pacific, and Atlantic, where the FGOALS_s produces the warmest SSTA in September-October and the coldest in February-

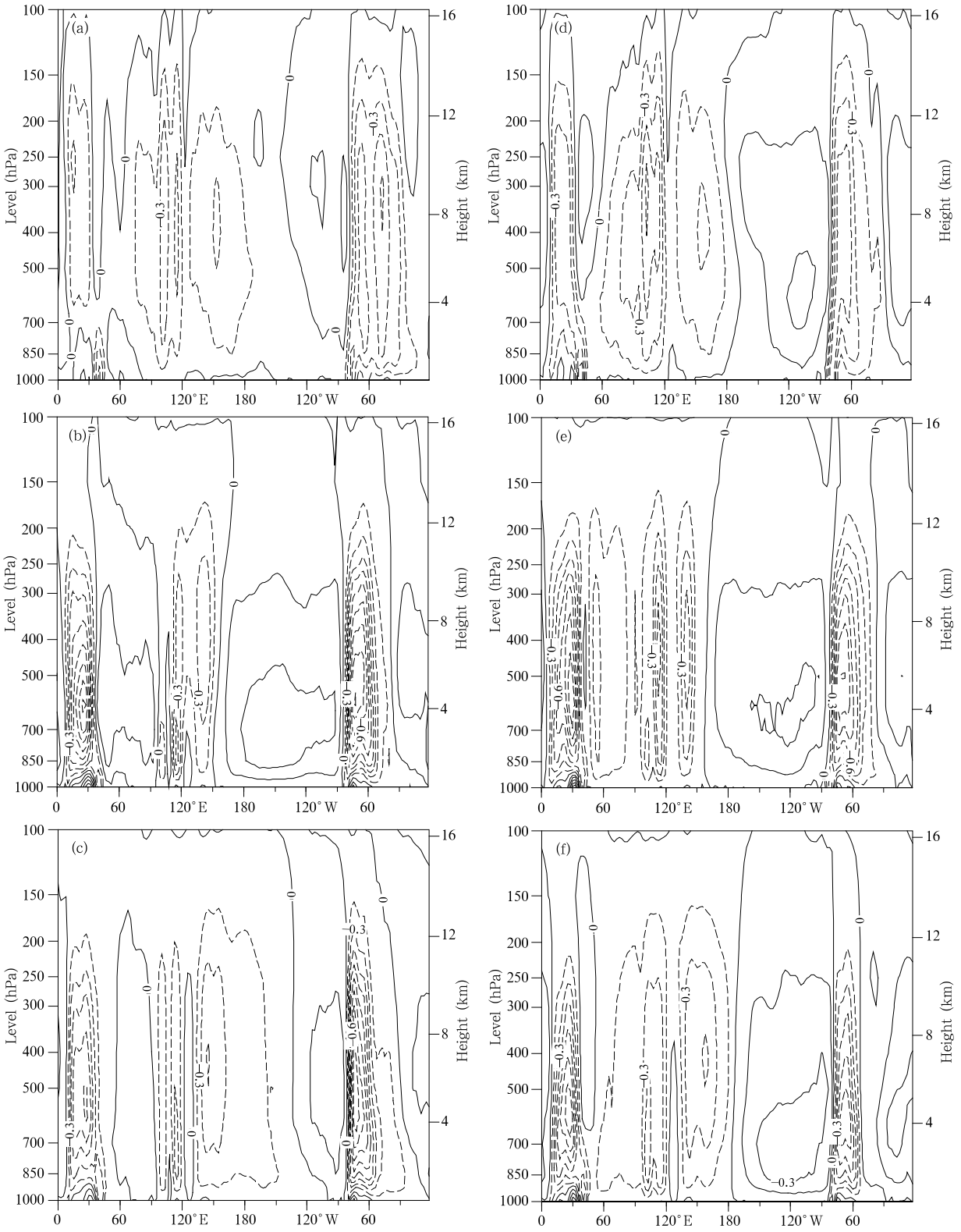

Fig. 7. Longitude-height diagrams of vertical velocity (Pa s^{-1}) for the equatorial belt (averaged from 5°S to 5°N) in boreal spring (April and May; left panels) and fall (October and November; right panels). (a, b), (c, d), and (e, f) are from observation, FGOAL_s, and SAMIL, respectively.

March.

Compared with the Pacific cold tongue region, the simulated SSTA over the eastern equatorial Pacific is warmer in boreal spring and colder in boreal fall. Hence, the simulated Walker circulation across the Pacific Ocean is enhanced in boreal spring but

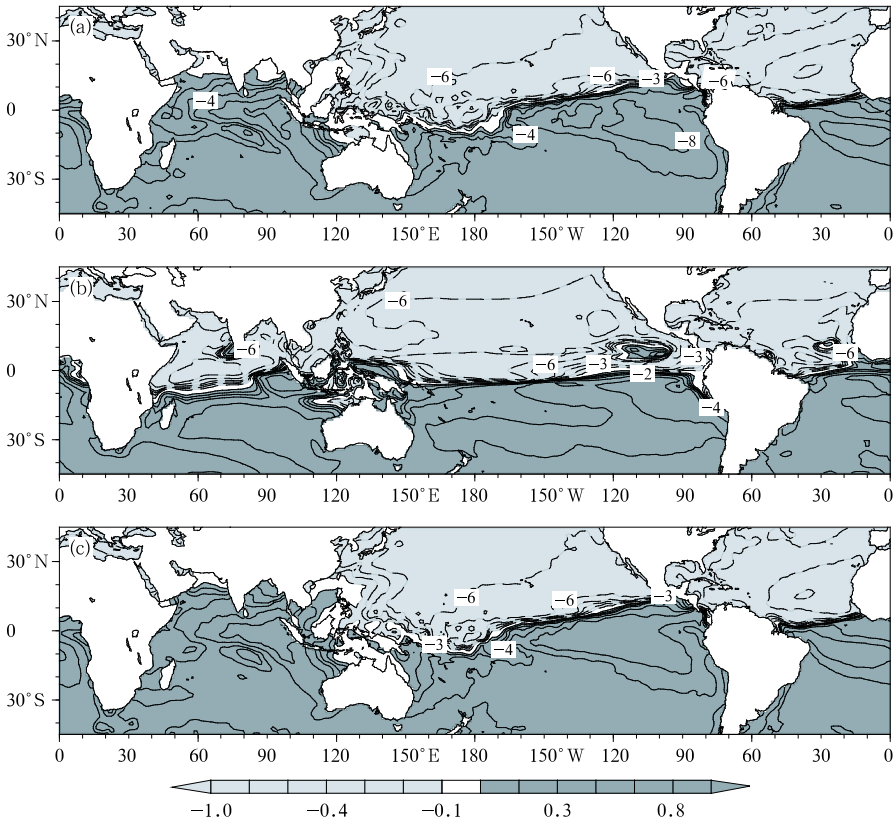

Fig. 8. Spatial distributions of correlation coefficients between PC2 and SST in (a) observation, (b) FGOALS_s, and (c) SAMIL. The darkly shaded areas denote positive values, while the lightly shaded negative values.

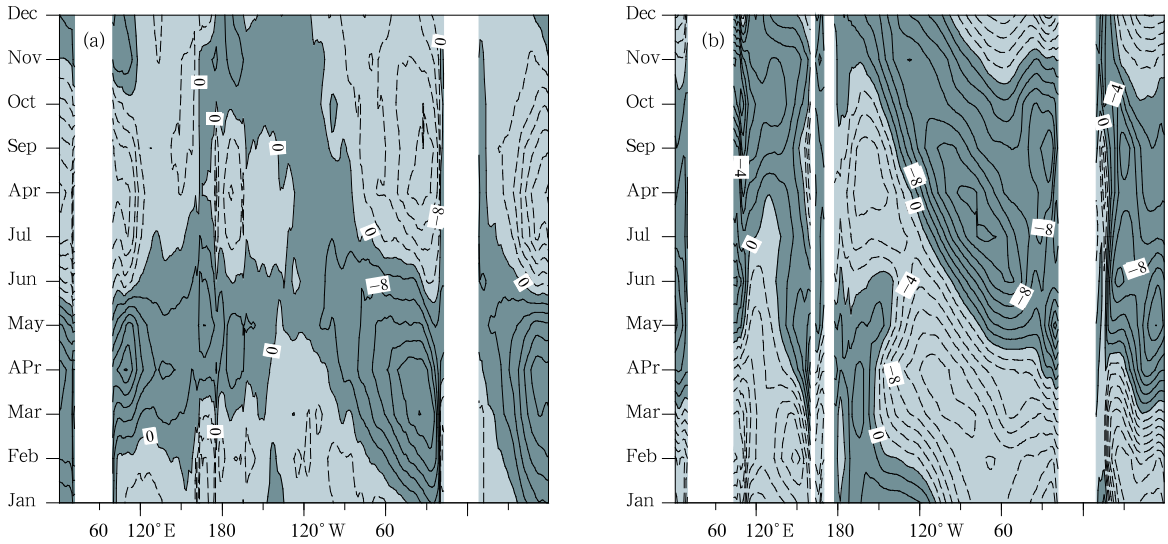

Fig. 9. Longitude-time diagrams of SST anomalies (°C; the departures of climatologically monthly mean from the long-term annual mean) for the equatorial belt (averaged form 5°S to 5°N) from (a) observation and (b) FGOALS_s. The darkly shaded areas denote positive values, while the lightly shaded negative values.

suppressed in fall, which weakens the spring-fall asymmetry. In the equatorial Indian Ocean, as a result of the simulated opposite phase of SSTA in spring and fall, the simulated Indian anti-Walker circulation is much stronger in boreal spring than in boreal fall, which also results in the stronger (weaker) ascent motion in boreal spring (fall) (Figs. 7b, e). Therefore, the deficiency of FGOALS_s in simulating the spring-fall asymmetry mode is associated with its poor performance in simulating the annual cycle of SST.

5. Conclusions

This paper evaluates the performance of LASG/IAP coupled general circulation model FGOALS_s in simulating the annual modes of the tropical precipitation. A comparison between the fully coupled and stand-alone AGCM simulations is used to discuss the impact of air-sea coupling processes on the simulation of annual cycle. Major results are summarized as follows:

(1) Previous studies indicated that the dominant modes of the annual variation of tropical precipitation are the monsoon mode and the spring-fall asymmetric mode (Wang and Ding, 2008). FGOALS_s reasonably simulates the primary features of the monsoon mode, such as the antisymmetry about the equator. However, the amplitude of the simulated monsoon mode is stronger than the observation in the Southern Hemisphere.

The CGCM shows a poor performance in simulating the spring-fall asymmetric mode. It may be associated with its deficiency in simulating the annual cycle of equatorial SST. In the observation, the spring-fall asymmetric mode is caused by the weaker amplitude of the Walker circulation in boreal spring relative to that in fall. The Walker circulation is forced by the gradients of zonal SST. Since the simulated SST annual cycles in boreal spring and fall over the equatorial Pacific Ocean and Indian Ocean are opposite to the observation, the simulated Walker circulation is stronger in boreal spring but weaker in boreal fall. The reduced difference of Walker circulation between spring and fall causes the poor simulation of the spring-fall asymmetric mode.

(2) The FGOALS_s realistically simulates the major monsoon domains including those of the Asian-Australian monsoon, North and South African monsoon, North and South American monsoon, etc. The annual cycle and strength of monsoon precipitation in these regions are close to the observation. The primary biases appear in the East Asian and western North Pacific monsoon regions. The simulated monsoon areas are significantly smaller than the observation. In addition, the intensity of the East Asian monsoon is weaker than the observation, and the phase evolution of the western North Pacific monsoon is not consistent with the observation.

(3) A comparison of the stand-alone AGCM run with the fully coupled run is carried out to explore the influence of air-sea coupling. The SAMIL tends to simulate heavier precipitation than the observation. The bias is reduced in the coupled run. The monsoon domains of the coupled model is closer to the observation than the SAMIL. Compared with SAMIL, FGOALS_s improves the simulation of North African, Australian monsoon domains and the annual cycle of North African monsoon. The main deficiencies of the coupled run include the bias in climatological mean precipitation in boreal spring and winter, spring-fall asymmetry mode, and the area size of the western North Pacific monsoon domain. The annual cycle of precipitation in all monsoon regions in the coupled run is worse than the stand-alone AGCM run, except for the North African monsoon. Therefore, the deficiency of FGOALS_s in the monsoon simulation arises not only from its atmosphere component, but also from the SST biases, especially the tropical SST biases. How to improve the performance of FGOALS_s in the simulation of SST annual cycle deserves a further study.

REFERENCES

Annamalai, H., J. M. Slingo, K. R. Sperber, and K. Hodges, 1999: The mean evolution and variability of Asian summer monsoon: Comparison of ECMWF and NCEP/NCAR reanalysis. *Mon. Wea. Rev.*, **127**, 1157–1186.

Bao Qing, Liu Yimin, Zhou Tianjun, et al., 2006: The sensitivity of the spectral atmospheric general circulation model of LASG/ IAP to the land process.

Chinese J. Atmos. Sci., **30**, 1077–1090. (in Chinese)

Biasutti, M., D. S. Battisti, and E. S. Sarachik, 2003: The annual cycle over the tropical Atlantic, South America, and Africa. *J. Climate*, **16**, 2491–2508.

Briegleb, B. P., et al., 2002: The sea ice simulation of the Community Climate System Model, Version two. NCAR Tech. Note, NCAR/TN-455+STR, 34.

Chang, C. P., Z. Wang, J. McBride, et al., 2005: Annual cycle of Southeast Asia-Maritime continent rainfall and the asymmetric monsoon transition. *J. Climate*, **15**, 287–301.

Chase, T. N., J. A. Knaff, R. A. Pielke Sr., et al., 2003: Changes in global monsoon circulations since 1950. *Natural Hazards*, **29**, 229–254.

Chen, T. C., J. M. Chen, and J. Pfaendtner, 1995: Low-frequency variations in the atmospheric branch of the global hydrological cycle. *J. Climate*, **8**, 92–107.

——, W. R. Huang, and E. S. Takle, 2004: Annual variation of midlatitude precipitation. *Notes and Correspondents*, **17**, 4291–4298.

Dai, A., 2006: Precipitation characteristics in eighteen coupled climate models. *J. Climate*, **19**, 4605–4630.

Dai Xingang, Chou Jifan, and Wu Guoxiong, 2002: The teleconnection relationship between Indian monsoon and East Asian summer circulation. *Acta Meteor. Sinica*, **60**, 544–552. (in Chinese)

Ferranti, L., J. M. Slingo, T. N. Palmer, and B. J. Hoskins, 1997: Relations between interannual and intraseasonal monsoon variability as diagnosed from AMIP integrations. *Quart. J. Roy. Meteor. Soc.*, **123**, 1323–1357.

Fu Congbin and Zeng Shaomei, 1997: Monsoon-the area where the variability of precipitation is most significant. *Chinese Science Bulletin*, **42**(21), 2306–2309. (in Chinese)

Gadgil, S., and G. Asha, 1992: Intraseasonal variation of the Indian summer monsoon. Part I: Observational aspects. *J. Meteor. Soc. Japan*, **70**, 517–527.

Hasternrath, S., and L. Heller, 1977: Dynamics of climatic hazards in northeast Brazil: Quart. *J. Roy. Meteor. Soc.*, **103**, 77–92.

——, and P. Lamb, 1978: On the dynamics and climatology of surface flow over the equatorial oceans. *Tellus*, **30**, 436–448.

Horel, J. D., 1982: On the annual cycle of the tropical Pacific atmosphere and ocean. *Mon. Wea. Rev.*, **110**, 1863–1878.

Jaeger, L., 1983: Monthly and areal patterns of mean global precipitation. *Variation in the Global Water Budget*. A. Street-Perrott et al., Eds., Reidel, 129–140.

Jin, X. Z., X. Zhang, and T. Zhou, 1999: Fundamental framework and experiments of the third generation of IAP/LASG World Ocean General Circulation Model. *Adv. Atmos. Sci.*, **16**, 197–215.

Jones, D., D. Collins, N. Nicholls, et al., 2004: A new tool for tracking Australia's climate variability and change. *Bulletin of the Australian Meteorological and Oceanographic Society*, **17**, 65–69.

Kalnay, E., and Coauthors, 1996: The NCEP/NCAR 40-year reanalysis project. *Bull. Amer. Meteor. Soc.*, **77**, 437–471.

Kripalani, R. H., A. Kulkarni, S. S. Sabade, et al., 2003: Indian monsoon variability in a global warming scenario. *Natural Hazards*, **29**, 189–206.

Lau, K. M., and P. J. Sheu, 1988: Annual cycle, QBO and Southern Oscillation in global precipitation. *J. Geophys. Res.*, **93**, 10975–10988.

——, and H. Y. Weng, 2002: Recurrent teleconnection patterns linking summertime precipitation variability over East Asia and North America. *J. Meteor. Soc. Japan*, **80**, 1309–1324.

Li, T., and S. G. H. Philander, 1996: On the annual cycle of the eastern equatorial Pacific. *J. Climate*, **9**, 2986–2998.

Liu, H., X. Zhang, W. Li, et al., 2004: An eddy-permitting oceanic general circulation model and its preliminary evaluations. *Adv. Atmos. Sci.*, **21**, 675–690.

Meehl, G. A., 1987: The annual cycle and interannual variability in the tropical Pacific and Indian Ocean regions. *Mon. Wea. Rev.*, **115**, 27–50.

Merle, J., M. Fieux, and P. Hisard, 1980: Annual signal and interannual anomalies of sea surface temperature in the eastern equatorial Atlantic Ocean. *Deep Sea Res.*, **26**, GATE suppl. II, 885–891.

Peizoto, J. P., and A. H. Oort, 1983: The atmospheric branch of the hydrological cycle and climate. *Variation in the Global Water Budget*. A. Street-Perrott et al., Eds., Reidel, 5–65.

Picaut, J., 1983: Propagation of the seasonal upwelling in the eastern equatorial Atlantic. *J. Phys. Oceanogy*, **13**, 18–37.

Rayner, N. A., E. B. Horton, D. E. Parker, et al., 1996: Version 2.2 of the global sea-ice and sea surface temperature dataset, 1903–1994. *Climate Research Technical Note*, **74**, 1–21.

Schreck, C. J. III, and F. H. M. Semazzi, 2004: Variability of the recent climate of eastern Africa. *Int. J. Climate*, **24**, 681–701.

Taylor, K. E., 2001: Summarizing multiple aspects of model performance in a single diagram. *J. Geophys. Res.*, **106**, 7183–7192.

Trenberth, K. E., D. P. Stepaniak, and J. M. Caron, 2000: The global monsoon as seen through the divergent atmospheric circulation. *J. Climate*, **13**, 3969–3993.

Vertenstein, M., K. Oleson, and S. Levis, 2002: CLM2.0 User's Guide. National Center for Atmospheric Research,

P.O. Box 3000, Boulder, CO, U. S. A., 1–36.

Wang, B., 1994: On the annual cycle in the tropical eastern Central Pacific. *J. Climate*, **7**, 1926–1942.

——, R. Wu, and K. Lau, 2001: Interannual variability of the Asian summer monsoon: Contrast between the Indian and the western North Pacific-East Asian monsoons. *J. Climate*, **14**, 4073–4090.

——, and H. Lin, 2002: Rainy season of the Asian-Pacific summer monsoon. *J. Climate*, **15**, 386–398.

——, and Q. Ding, 2006: Changes in global monsoon precipitation over the past 56 years. *Geophys. Res. Lett.*, **33**, L06711.

——, and Q. Ding, 2008: The global monsoon: major modes of annual variation in tropical precipitation and circulation. *Dynamics of Atmospheres and Oceans*, **44**, 165–183.

Wang Zaizhi, Yu Rucong, Bao Qing, et al., 2007: A comparison of the atmospheric circulations simulated by the FGOALS_s and SAMIL. *Chinese J. Atmos. Sci.*, **31**, 202–213. (in Chinese)

Webster, P. J., T. Palmer, M. Yanaiet, et al., 1998: Monsoons: Processes, predictability and the prospects for prediction. *J. Geophys. Res.*, **103**, 14451–14510.

Wyrtki, K., 1965: The annual and semiannual variations of SST in the North Pacific Ocean. *Limnol. Oceanogr.*, **10**, 307–313.

——, and G. Mayers, 1976: The trade wind field over the Pacific Ocean, *J. Metero.*, **15**, 698–704.

Xie, P. P., and P A. Arkin, 1997: Global precipitation: A 17-year monthly analysis based on gauge observations, satellite estimates and numerical model outputs. *Bull. Amer. Meteor. Soc.*, **78**, 2539–2558.

Yu, R. C., and T. Zhou, 2007: Seasonality and three-dimensional structure of the interdecadal changes in the East Asian monsoon. *J. Climate*, **20**, 5344–5355.

Zhou Tianjun, Zhang Xuehong, and Wang Shaowu, 1999: The air-sea freshwater exchange derived from NCEP/NCAR reanalysis data. *Acta Meteor. Sinica*, **57**, 264–282. (in Chinese)

——, Yu Rucong, Wang Zaizhi, et al., 2005a: *Atmosphere Circulation Model SAMIL and the Fully Coupled Model FGOALS_s.* China Meteorological Press, Beijing, 288 pp. (in Chinese)

——, Wang Zaizhi, Yu Rucong, et al., 2005b: The climate system model FGOALS_s using LASG/IAP spectral AGCM SAMIL as its Atmospheric component. *Acta Meteor. Sinica*, **63**, 702–715. (in Chinese)

Zhou, T. J., and R. Yu, 2006: Twentieth-century surface air temperature over China and the globe simulated by coupled climate models. *J. Climate*, **19**, 5843–5858.

——, ——, H. Li, et al., 2008a: Ocean forcing to changes in global monsoon precipitation over the recent half century. *J. Climate*, **21**, 3833–3852.

——, L. Zhang, and H. Li, 2008b: Changes in global land monsoon area and total rainfall accumulation over the last half century. *Geophys. Res. Lett.*, **35**, L16707.

——, B. Wu, X. Wen, et al., 2008c: A fast version of LASG/IAP climate system model and its 1000-year control integration. *Adv. Atmos. Sci.*, **25**(4), 655–672.